Early View publication on www.interscience.wiley.com
(issue and page numbers not yet assigned;
citable using Digital Object Identifier – **DOI**)

phys. stat. sol. (c), 1–3 (2008) / **DOI** 10.1002/pssc.200778482

physica status solidi c
www.pss-c.com
current topics in solid state physics

Band gap and effective electron mass of cubic InN

P. Schley[1,*], C. Napierala[1], R. Goldhahn[1], G. Gobsch[1], J. Schörmann[2], D. J. As[2], K. Lischka[2], M. Feneberg[3], K. Thonke[3], F. Fuchs[4], and F. Bechstedt[4]

[1] Institute of Physics, Technical University Ilmenau, PF 100565, 98684 Ilmenau, Germany
[2] Department Physics, University Paderborn, Warburger Str. 100, 33098 Paderborn, Germany
[3] Institute of Semiconductor Physics, University of Ulm, 89069 Ulm, Germany
[4] Institute of Solid State Theory and Optics, Friedrich-Schiller-University Jena, Max-Wien-Platz 1, 07743 Jena, Germany

Received 6 September 2007, accepted 17 December 2007
Published online 27 March 2008

PACS 71.20.Nr, 78.20.Ci, 78.30.Fs, 78.66.Fd, 81.15.Hi

* Corresponding author: e-mail pascal.schley@tu-ilmenau.de, Phone: +49-3677-693210, Fax: +49-3677-693173

We succeeded in growing single crystalline c-InN films on 3C-SiC substrate with a c-GaN buffer layer by MBE. Spectroscopic ellipsometry is applied in order to determine the complex dielectric function for cubic InN from mid-infrared into the visible spectral region. The high electron densities above $10^{19}\,\mathrm{cm}^{-3}$ cause pronounced Burstein-Moss shifts at the gap. Taking into account the non-parabolicity and the filling of the conduction band, data analysis yields renormalized band edges between 0.430 and 0.455 eV. Including carrier-induced band-gap renormalization we estimate a zero-density band gap of ∼0.596 eV for c-InN with a corresponding effective electron mass of 0.041 m_0 at the Γ point of the Brillouin zone.

1 Introduction InN has attracted much interest due to the recent band gap revision for the hexagonal (h-) polymorph. Zero electron density values at room temperature (RT) between 0.65 [1,2] and 0.68 eV [3,4] were reported depending on the approaches used for modeling the spectra around the absorption edge and whether carrier-induced band-gap renormalization (BGR) and Burstein-Moss shift (BMS) were taken into account. An additional uncertainty arises from the determination of the bulk electron concentration (N_e) in the presence of a strong surface accumulation layer [5].

Much less is known about the cubic counterpart (c-InN). Calculations predict an even lower band gap between 0.53 and 0.65 eV [6–8]. Only recently high-quality c-InN layers became available [9]. The current paper presents a detailed analysis of their optical properties.

2 Experimental Nominally undoped c-InN films with 127 nm (sample A), 122 nm (B), and 75 nm (C) thickness were grown by rf plasma-assisted molecular beam epitaxy at temperatures of 434°C, 431°C, and 419°C, respectively. Prior to the growth, thick c-GaN buffer layers (∼600 nm, $N_e \approx 2 \times 10^{17}\mathrm{cm}^{-3}$) were deposited at 720°C on the (001)-oriented 3C-SiC substrates ($N_e \approx 5 \times 10^{17}\mathrm{cm}^{-3}$). Further growth details have been published elsewhere [9].

The high-resolution X-ray diffraction studies yielded the following results. The $\omega - 2\theta$ scans, displayed in Fig. 1, show Bragg peaks at 35.8°, 39.9°, and 41.3° corresponding to c-InN (002), c-GaN (002), and 3C-SiC (002), respec-

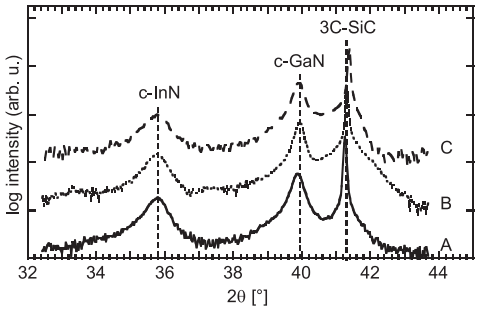

Figure 1 (002) reflection $\omega - 2\theta$ scans recorded for the investigated InN samples. The data have been vertically shifted for the sake of clarity.

tively. As expected, the c-InN peaks become sharper with increasing layer thickness. The lattice constants obtained from the $\omega - 2\theta$ scans amount to (5.01 ± 0.01) Å which is close to the value of 4.986 Å reported in Refs. [10, 11]. The analysis of reciprocal space maps yielded hexagonal inclusions of only 11% (A), 10% (B), and 5% (C), respectively.

A Fourier-transform-based ellipsometer with a spectral resolution of $1\,\mathrm{cm}^{-1}$ was used to investigate the optical properties in the mid-IR range (350–2000 cm^{-1}). From the near-IR to visible region, the ellipsometric parameters Ψ and Δ were measured by a rotating-analyzer ellipsometer; the spectral resolution was 10 meV. The real (ε_1) and imaginary part (ε_2) of the complex dielectric function (DF) ($\bar{\varepsilon} = \varepsilon_1 + i\varepsilon_2$) were obtained by fitting experimental data using a multi-layer model c-InN/c-GaN/3C-SiC including surface roughness. The Photoluminescence (PL) at 10 K was excited by the 514 nm line of an Ar^+-ion laser and detected by a liquid-nitrogen cooled InSb photodiode.

3 Results and discussion Figure 2a shows the imaginary parts close to the band gap as well as the corresponding PL spectra at 10 K. The shape of ε_2 is very similar to the behavior found for degenerate h-InN [4], a sharp increase is followed by a plateau. The onset of absorption is obviously influenced by the carrier-induced BMS. Applying the fitting procedure presented in Ref.[4] allows the unambiguous determination of the Fermi energy E_F from the ε_2 data as indicated in Fig. 2a. The Stokes shift between the PL emission maximum (found at ∼0.5 eV for all samples) and E_F increases from sample A to C indicating increasing N_e. It influences also the shape of ε_1 which is demonstrated in Fig. 2b. The peak position shifts with N_e due to the Kramers-Kronig consistency of ε_1 and ε_2, and the high-frequency dielectric constant ε_∞ (extrapolation to zero photon energy) becomes lower. The spectral dependence of ε_1 below the gap can be represented by an analytical expression [12]. In the case of $\hbar\omega \to 0$, one obtains the values for ε_∞ which are listed in Table 1.

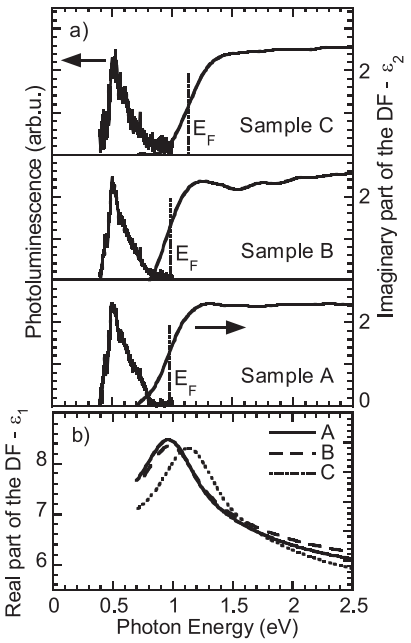

Figure 2 a) PL spectra at $T = 10$ K and imaginary parts of the DF at RT for c-InN. The PL curves have been normalized to equal amplitude for the sake of clarity, the transition energies at the Fermi wave vector are indicated by E_F. The real parts of the DF are shown in b).

Table 1 Determined IR data such as phonon frequencies, plasma frequencies, and broadening parameters as well as electron concentrations and high-frequency dielectric constants of c-InN. The optical effective masses $m^*(N_e)$ are also given.

Sample	ω_TO [cm^{-1}]	ω_p [cm^{-1}]	γ_p [cm^{-1}]	N_e [$10^{19}\mathrm{cm}^{-3}$]	$\varepsilon_\infty(N_e)$	$m^*(N_e)$ /m_0
A	468.9	2025	167	2.1	6.97	0.067
B	469.3	2061	190	2.2	6.95	0.068
C	470.0	2599	212	3.8	6.64	0.076

Determination of the zero-density band gap of c-InN from the E_F data becomes possible with the approach recently applied to h-InN [4]. The electron densities as input parameters are determined by analyzing the free carrier excitations in the IR as obtained from SE [13]. The DFs of the 3C-SiC, c-GaN and c-InN layers in the mid-IR range were analyzed by a factorized expression for anharmonic coupling effects between free-carrier plasmons and longitudinal-optical (LO) phonons . The adjustable sample fit parameters are the transversal-optical (TO) lattice mode (ω_TO) and the plasma frequency (ω_p) as well as the corresponding broadening parameters. The LO mode was kept fixed to $588\,\mathrm{cm}^{-1}$ for all samples [12]. The needed ε_∞ values for each c-InN film are taken from Table 1.

Figure 3 shows the obtained ellipsometric Ψ (a) and Δ (b) spectra of sample C as an example. Measured and modeled data excellently agree with each other. The positions of the TO- and LO-phonons are labeled by arrows. Note that by means of the analytical DF the measured reflectance spectrum depicted in Fig. 3c can be well reproduced. It emphasizes the accuracy of the fit.

The TO mode for sample C was detected at $470.0\,\mathrm{cm}^{-1}$. We obtain a plasma frequency of $2599\,\mathrm{cm}^{-1}$. The results of IR-SE data analysis of all samples are summarized in Table 1. In order to determine the electron concentration from ω_p we use the following modified equation [14]:

$$\omega_\mathrm{p}^2 = \frac{N_e e^2}{\varepsilon_0 \varepsilon_\infty m^*(N_e)}\,, \qquad (1)$$

where e is the electrical unity charge and ε_0 represents the vacuum permittivity. The average effective mass $m^*(N_e)$ accounts for the nonparabolic dispersion of a conduction

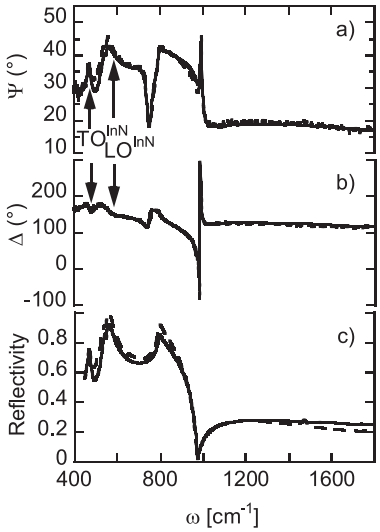

Figure 3 Measured (dashed lines) and modeled (solid lines) Ψ (a) and Δ (b) spectra at an angle of incidence of 65° as well as the IR reflectance spectrum c) for sample C. The position of the TO and LO phonon modes are labeled by arrows.

band (CB) with electron density N_e:

$$\frac{1}{m^*(N_e)} = \frac{1}{12\pi^3\hbar^2 N_e}\int d\mathbf{k}\frac{\partial^2 E_\mathrm{c}}{\partial k^2} f(E_\mathrm{c})\,, \qquad (2)$$

where $f(E_\mathrm{c})$ is the Fermi distribution function and E_c denotes the dispersion of the CB. The latter one is given by Kane's two-band $\mathbf{k}\cdot\mathbf{p}$ model inserting the renormalized band gap (E_ren) instead of the fundamental band gap E_0 [4]. The dispersion for c-InN is well described by a value of $E_\mathrm{P} = 14\,\mathrm{eV}$ [12]. Furthermore, only the quantity $N_e/m^*(N_e)$ can be determined from the plasma frequency [15]. So the problem has to be solved self-consistently using Eqs. (1) and (2) in this article and Eqs. (4) – (6) of Ref. [4]. With the values obtained for the electron densities and the averaged effective masses (see Table 1), E_F of the c-InN films can now be analyzed in analogy to h-InN [4] which is briefly discussed for sample C.

For the evaluation of the BMS [$\Delta E_\mathrm{cv}(k_\mathrm{F}) = \Delta E_\mathrm{c}(k_\mathrm{F}) - \Delta E_\mathrm{v}(k_\mathrm{F}) = E_\mathrm{F} - E_\mathrm{ren}$), the curvatures of the CB and valence band (VB) are needed . The VB is described by a parabolic approximation with an effective mass for the holes of $m_h = 0.5m_0$. The shape of the CB is expressed by the dispersion mentioned above. Starting from the experimentally determined VB-CB splitting at the Fermi wave vector k_F (Fermi energy E_F) of 1.130 eV and taking into account $\Delta E_\mathrm{cv}(k_\mathrm{F}) = 700\,\mathrm{meV}$, we obtain the energy of the renormalized band gap ($E_\mathrm{ren} = 0.430\,\mathrm{eV}$). Using a static dielectric constant ε_r of 12.3 [12] for c-InN, the band-gap renormalization (Δ_BGR) for sample C amounts to -173 meV for an electron concentration of $3.8\times10^{19}\,\mathrm{cm}^{-3}$. Finally, it results in an estimated zero-density band gap of 0.603 eV with a corresponding effective electron mass of $0.041\,m_0$ at the Γ point of the Brillouin zone. A detailed analysis for the two other samples can be found elsewhere [12]; values for E_0 of 0.595 (A) and 0.591 eV (B) were found. Due to the uncertainty of the BGR formula, the E_0 values represent the upper limit, slightly lower gaps might be possible as well.

4 Conclusion The dielectric function of cubic InN layers in the mid-IR spectral region as well as around the absorption edge has been analyzed. The determination of the plasma frequency from IR data provides the electron concentration of the films. The high-frequency dielectric constant decreases with increasing electron concentration. Taking into account band-filling and non-parabolicity of the conduction band for the analysis of ε_2 data in the vicinity of the band gap, we estimate for c-InN a zero carrier density band gap of 0.596 eV and an electron effective mass of $0.041\,m_0$ at the conduction band minimum.

Acknowledgements The authors would like to thank H. Nagasawa and M. Abe from HOYA Corporation, SiC Development Center, for supplying the 3C-SiC substrates.

References

[1] A. Kasic, E. Valcheva, B. Monemar, H. Lu, and W. J. Schaff, Phys. Rev. B **70**, 115217 (2004).
[2] G. Koblmüller, C. S. Gallinat, S. Bernardis, J. S. Speck, G. D. Chern, E. D. Readinger, H. Shen, and M. Wraback, Appl. Phys. Lett. **89**, 071902 (2006).
[3] W. Walukiewicz, J. W. Ager III, K. M. Yu, Z. Liliental-Weber, J. Wu, S. X. Li, R. E. Jones, and J. D. Denlinger, J. Phys. D: Appl. Phys. **39**, R83 (2006).
[4] P. Schley, R. Goldhahn, A. T. Winzer, G. Gobsch, V. Cimalla, O. Ambacher, H. Lu, W. J. Schaff, M. Kurouchi, Y. Nanishi, M. Rakel, C. Cobet, and N. Esser, Phys. Rev. B **75**, 205204 (2007).
[5] L. F. J. Piper, T. D. Veal, I. Mahboob, C. F. McConville, H. Lu, and W. J. Schaff, Phys. Rev. B **70**, 115333 (2004).
[6] P. Rinke, M. Scheffler, A. Qteish, M. Winkelnkemper, D. Bimberg, and J. Neugebauer, Appl. Phys. Lett. **89**, 161919 (2006).
[7] J. Furthmüller, P. H. Hahn, F. Fuchs, and F. Bechstedt, Phys. Rev. B **72**, 205106 (2005).
[8] D. Bagayoko, L. Franklin, and G. L. Zhao, J. Appl. Phys. **96**, 4297 (2004).
[9] J. Schörmann, D. J. As, K. Lischka, P. Schley, R. Goldhahn, S. F. Li, W. Löffler, M. Hetterich, and H. Kalt, Appl. Phys. Lett. **89**, 261903 (2006).
[10] V. Cimalla, J. Pezoldt, G. Ecke, R. Kosiba, O. Ambacher, L. Spieß, G. Teichert, H. Lu, and W. J. Schaff, Appl. Phys. Lett. **83**, 3468 (2003).
[11] M. F. Wu, S. Q. Zhou, A. Vantomme, Y. Huang, H. Wang, and H. Yang, J. Vac. Sci. Technol. A **24**, 275 (2006).
[12] P. Schley, R. Goldhahn, C. Napierala, G. Gobsch, J. Schörmann, D. J. As, K. Lischka, M. Feneberg, and K. Thonke, Semicond. Sci. Technol., submitted.
[13] A. Kasic, M. Schubert, S. Einfeldt, D. Hommel, and T. E. Tiwald, Phys. Rev. B **62**, 7365 (2000).
[14] M. P. Hasselbeck and P. M. Enders, Phys. Rev. B **57**, 9674 (1998).
[15] Y. Ishitani, T. Ohira, X. Wang, S. B. Che, and A. Yoshikawa, Phys. Rev. B **76**, 045206 (2007).